(Received 13 September 2025, Accepted 13 November 2025, Scheduled 23 November 2025)

A Compact Wideband 4-Port MIMO Antenna with Novel C-Shaped Radiators and Enhanced Isolation Characteristics

Pandillapalli Janardhana Reddy[1,*] and Gummadi Kameswari[2]

[1]Department of ECE, JNTUA College of Engineering, Ananthapuramu, A.P, India
[2]Department of ECE, NBKR Institute of Science and Technology, Nellore, A.P, India

ABSTRACT: A compact four-element MIMO antenna with dimensions $40 \times 32 \times 1.2\,\text{mm}^3$ is presented. The design employs stylized C-shaped radiators with slanted edges and a shared defected ground plane integrated with folded stubs to enhance impedance matching and bandwidth. Fabricated on an RT5880 substrate ($\varepsilon_r = 2.2$, $\tan\delta = 0.0009$), the antenna achieves an ultra-wide operating range of 4.24–19.70 GHz with inter-element isolation above 20 dB. Diversity metrics, including envelope correlation coefficient (< 0.02), diversity gain (≈ 10 dB), channel capacity loss (< 0.0325 bits/s/Hz), and total active reflection coefficient (-12 to -24 dB), are verified through simulation and measurement, confirming robust MIMO characteristics. Owing to its wideband operation and high isolation, the antenna is suitable for sub-6 GHz 5G NR (n79: 4.4–5.0 GHz), WLAN/Wi-Fi (5.15–5.825 GHz), X-band navigation and radar (8–12 GHz), and Ku-band satellite communication (12–14.5 GHz).

1. INTRODUCTION

Ultra-wideband (UWB) technology has emerged as a promising solution for high-speed, low-power, and short-range wireless communication systems. UWB antennas, with their ability to operate over a broad frequency range, are widely adopted in radar, imaging, and high-data-rate networks. In multi-port configurations, they also provide spatial and pattern diversity, thereby enhancing channel capacity and link reliability in multiple-input multiple-output (MIMO) systems [1, 2].

Several UWB-MIMO antennas have been reported. In [3], a differential U-shaped feed with a stepped-slot radiator introduced band-rejection capability, while [4] achieved dual notches using T-shaped parasitic elements and inverted U-shaped slots. A dual-port antenna with A-shaped slots enabled 4–21 GHz operation in [5], whereas slot-loaded monopoles with a defected ground extended bandwidth to 20 GHz and improved compactness through orthogonal placement [6]. Characteristic mode analysis with a swastik-shaped ground stub improved isolation in [7], and a fan-shaped decoupling structure enabled 2–11.08 GHz operation in [8].

Isolation improvement has also been pursued through radiator and ground-plane modifications. Orthogonal spade-shaped radiators with T-shaped strips and rhombic slots improved isolation in [9], while bifurcated arrow-shaped parasitics enhanced diversity in [10]. A circular design with Y-shaped stubs maintained isolation below -18 dB [11]. Ground-plane extensions and parasitic stubs enabled wideband operation in [12, 13], though with larger footprints and moderate coupling suppression. Compact designs [14, 15] often suffered from isolation above -15 dB, while later works [16–19] achieved compactness at the cost of complex geometries. An octagonal radiator with parasitic stubs also improved isolation but added structural complexity [20].

More advanced approaches include corrugated ground planes with zigzag slots and U-shaped strips achieving > 20 dB isolation [21], T-shaped defected grounds with cross slots [22], and metamaterial-based methods [23] attaining isolation better than -25 dB. A four-element octagonal array with orthogonal polarization provided > 20 dB isolation [24]. Other designs used beveled radiators with L-shaped slots [25] or combined T- and L-shaped stubs with U-shaped slots for triple notches [26].

Compact, high-isolation UWB-MIMO antennas have also been proposed. In [27], slot insertion and feedline modification extended the bandwidth from 4.08–5.63 to 3.18–6 GHz while a T-shaped strip suppressed coupling. A semicircular disc-based four-port array with reverse slots and decoupling structures further improved impedance matching [28]. Collectively, these works highlight the ongoing effort toward compact UWB-MIMO antennas with wideband coverage and high isolation.

The proposed UWB-MIMO antenna employs a simple C-shaped radiator excited by a tapered microstrip feedline, which extends the current path to generate multiple resonances while maintaining compactness. Stepwise ground-plane modifications using a defected ground, parallel stubs, and a connecting strip ensure isolation better than -22 dB across 4.24–19.70 GHz. The antenna demonstrates superior diversity performance (ECC < 0.02, DG ≈ 9.97 dB, CCL < 0.325 bits/s/Hz, and TARC < -12 dB), providing an efficient and fabrication-friendly solution compared with more complex UWB-MIMO designs.

* Corresponding author: Pandillapalli Janardhana Reddy (janardhanreddy-1991@gmail.com).

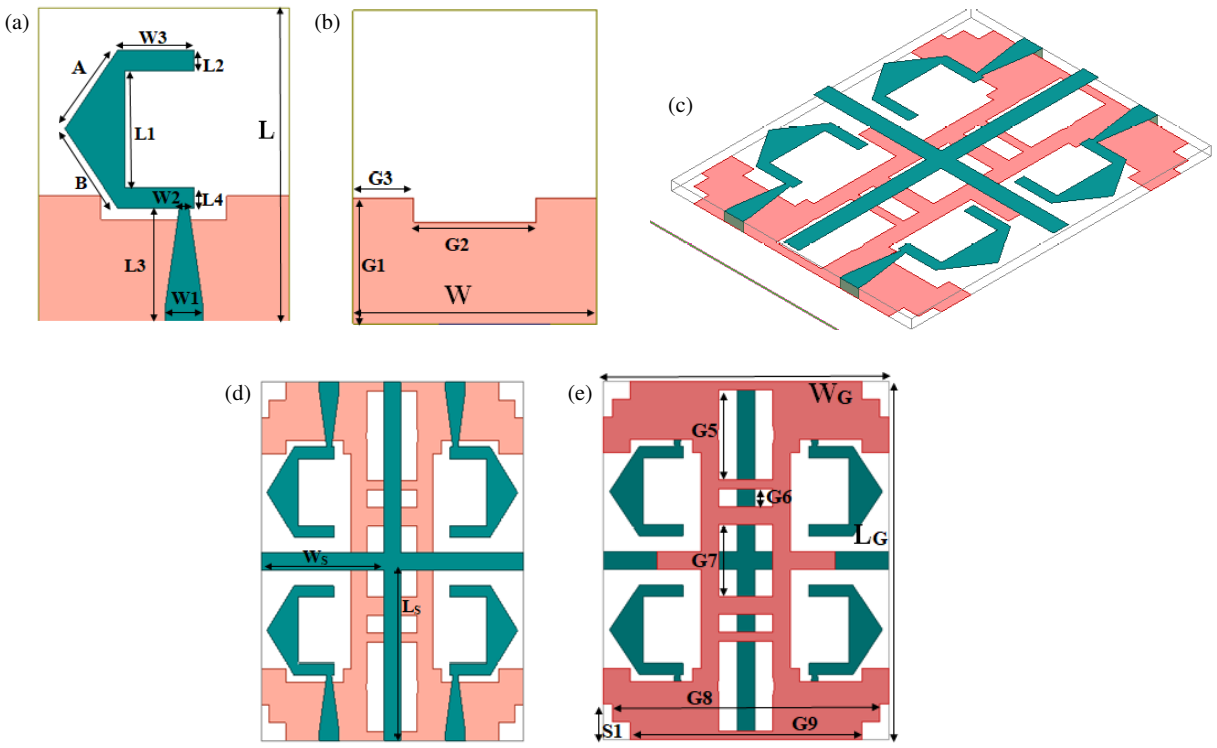

FIGURE 1. Basic antenna: (a) Top view, (b) Bottom view. Four-port antenna, (c) 3-D view of the MIMO antenna, (d) Top view, (e) Bottom view.

The rest of this paper is organized as follows. Section 2 describes the design and geometry of the proposed single-element and four-port MIMO antenna. Section 3 presents the simulated and measured performance metrics, while Section 4 concludes the work with key findings.

2. ANTENNA GEOMETRY AND DESIGN

The geometry of the proposed single-element antenna and four-port MIMO configuration is shown in Fig. 1. Figs. 1(a) and 1(b) illustrate the top and bottom views of the single radiator, while Figs. 1(c) and 1(d) show the corresponding MIMO design. The antenna is fabricated on an RT/Duroid 5880 substrate ($\varepsilon_r = 2.2$, thickness $= 1.2$ mm). The detailed dimensions are listed in Table 1.

TABLE 1. Design parameters of the proposed single element and four-port MIMO antenna (Corresponding to Fig. 1).

Parameters	L	W	$L1$	$L2$	$L3$	$L4$
Value (mm)	20	16	7.5	1.3	7.25	1.3
Parameters	$W1$	$W2$	$W3$	A	B	$G1$
Value (mm)	2.5	0.6	4.5	6	6	8
Parameters	$G2$	$G3$	L_G	W_G	L_S	W_S
Value (mm)	8	4	40	32	19	15
Parameters	$G6$	$G7$	$G8$	$G9$	$S1$	$G5$
Value (mm)	2	8	30	26	4	10

The fundamental resonance of the single C-shaped radiator can be approximated using the half-wavelength relation given in (1):

$$f_{res} \approx \frac{c}{2L_{eff}\sqrt{\varepsilon_{eff}}} \tag{1}$$

where "c" is the speed of light, L_{eff} the effective length of the C-shaped strip, and ε_{eff} the effective permittivity of the substrate. For the RT/Duroid 5880 substrate ($\varepsilon_r = 2.2$, $h = 1.2$ mm and $W \approx 2.5$ mm),

$$\varepsilon_{eff} = \frac{\varepsilon_r + 1}{2} + \frac{\varepsilon_r - 1}{2}\frac{1}{\sqrt{1 + 12\left(\frac{h}{w}\right)}} \approx 1.83 \tag{2}$$

Considering the radiator's effective length $L_{eff} \approx 15.8$ mm (sum of vertical arms and slanted edges), the first-order resonance frequency can be obtained from (3)

$$f_{res} \approx \frac{3 \times 10^8}{2 \times 15.8 \times 10^{-3} \times \sqrt{1.83}} \approx 7.0\,\text{GHz} \tag{3}$$

which lies within the reported operating band (4.24–19.70 GHz). Higher-order resonances, together with the perturbation introduced by the defected ground structure (DGS), contribute to the wideband response.

The C-shaped radiator follows a half-wavelength resonance model, while the DGS operates as an LC-resonator by perturbing the ground current path. Despite being based on different mechanisms, the two effects complement each other to produce the observed wideband performance.

The optimization process of the single-element antenna and its return loss characteristics are shown in Figs. 2(a)–2(e), labeled as Phase 1–Phase 4. In Phase 1, a basic rectangular patch

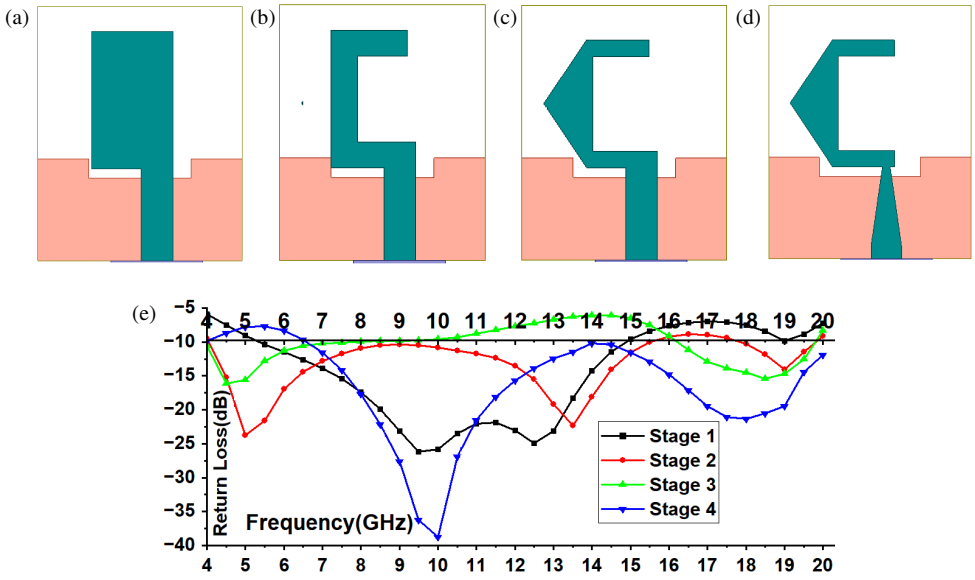

FIGURE 2. Evaluation metrics for the proposed antenna. (a) Phase 1, (b) Phase 2, (c) Phase 3, (d) Phase 4, (e) S_{11} parameters of each phase.

($10.8 \times 6.4\,\text{mm}^2$) with a defected ground structure exhibited poor impedance matching. Phases 2 and 3 introduced structural modifications to the patch, significantly improving impedance response. In Phase 4, a tapered impedance line replaced the stepped line, further enhancing matching across the desired bandwidth. These progressive changes collectively enabled the required wideband performance, as illustrated in Fig. 2(e).

The key design parameters were systematically optimized, with the corresponding parametric analysis shown in Figs. 3(a)–3(g). Variations in feed length ($L3$), extended patch length ($L2$), radiating patch length ($L1$), feed widths ($W1, W2$), extended patch width ($W3$), and ground-plane slots ($G1, G2$) were found to significantly affect antenna performance.

Figures 3(a)–3(c) show that the feed length ($L1$) and patch lengths ($L2, L3$) strongly affect impedance matching in the 6–12 GHz range. The optimal configuration ($L1 = 7.5\,\text{mm}$, $L2 = 1.3\,\text{mm}$, $L3 = 7.25\,\text{mm}$) improved impedance characteristics, where increasing $L1$ lowered the resonant frequency, and reducing $L2, L3$ shifted higher-order resonances upward for wideband matching.

Figures 3(d)–3(f) demonstrate that feedline widths (W_1, W_2) and the extended patch width ($W3$) mainly influence the 12–16 GHz band. The configuration ($W1 = 2.5\,\text{mm}$, $W2 = 0.6\,\text{mm}$, $W3 = 4.5\,\text{mm}$) yielded optimal mid-band performance, though with reduced low-frequency effectiveness. Here, $W1$ controls input reactance; $W2$ improves feed coupling; and $W3$ adjusts capacitive loading for resonance tuning.

As shown in Fig. 3(g), ground-plane slot lengths ($G1, G2$) also influence isolation and bandwidth. Optimal results were obtained at $G1 = G2 = 8\,\text{mm}$, where slot tuning redistributed surface currents, thereby reducing coupling and improving matching.

The far-field performance of the single element is analyzed at 10 GHz. Fig. 4(a) shows a directional pattern with a gain of 4.8 dB. The gain and efficiency across the band are given in Figs. 4(b) and 4(c), where the gain varies from 1.2 to 7.8 dB (peaking at 17 and 19 GHz), and efficiency remains 78–87.8%. These results validate the radiator's suitability for wideband operation and provide the basis for developing the proposed four-element MIMO configuration.

2.1. Four Port MIMO Antenna Configuration

According to Shannon's theorem, channel capacity increases with bandwidth and transmission power. However, spectrum limitations and regulated power levels restrict achievable data rates. To overcome this, multiple transmitter and receiver antennas are employed. Building on the single-element UWB antenna, the design was extended to a four-element MIMO configuration.

2.1.1. Evolution of MIMO Antenna

The progression of the four-element MIMO antenna is shown in Figs. 5(a)–5(c), aimed at improving isolation and impedance matching. Three design stages, Ant-1 through Ant-3, are considered, with their corresponding S-parameter responses and surface current distributions presented in Fig. 6.

A comparative analysis of three antenna configurations, evaluated through the S-parameters (S_{11}, S_{12}, S_{13}, S_{14}), shows distinct performance. All designs follow a parallel layout with 15.4 mm element spacing ($\approx 0.154\lambda$ at 3.0 GHz) and occupy a compact footprint of $40 \times 32 \times 1.2\,\text{mm}^3$.

As shown in Figs. 6(a)–6(d), Ant-1 achieves good impedance matching up to 12 GHz but suffers from strong mutual coupling. Ant-2, with parallel ground stubs, slightly improves matching and reduces coupling in the 13.5–15.5 GHz band. Ant-3, employing cross-placed stubs, provides the best results, with isolation better than -40 dB at 10.5 and 12 GHz and $S_{11} < -10$ dB across 13.5–15.5 GHz. These trends are confirmed by the surface current distributions in Figs. 6(e)–6(g) at 8.5 GHz.

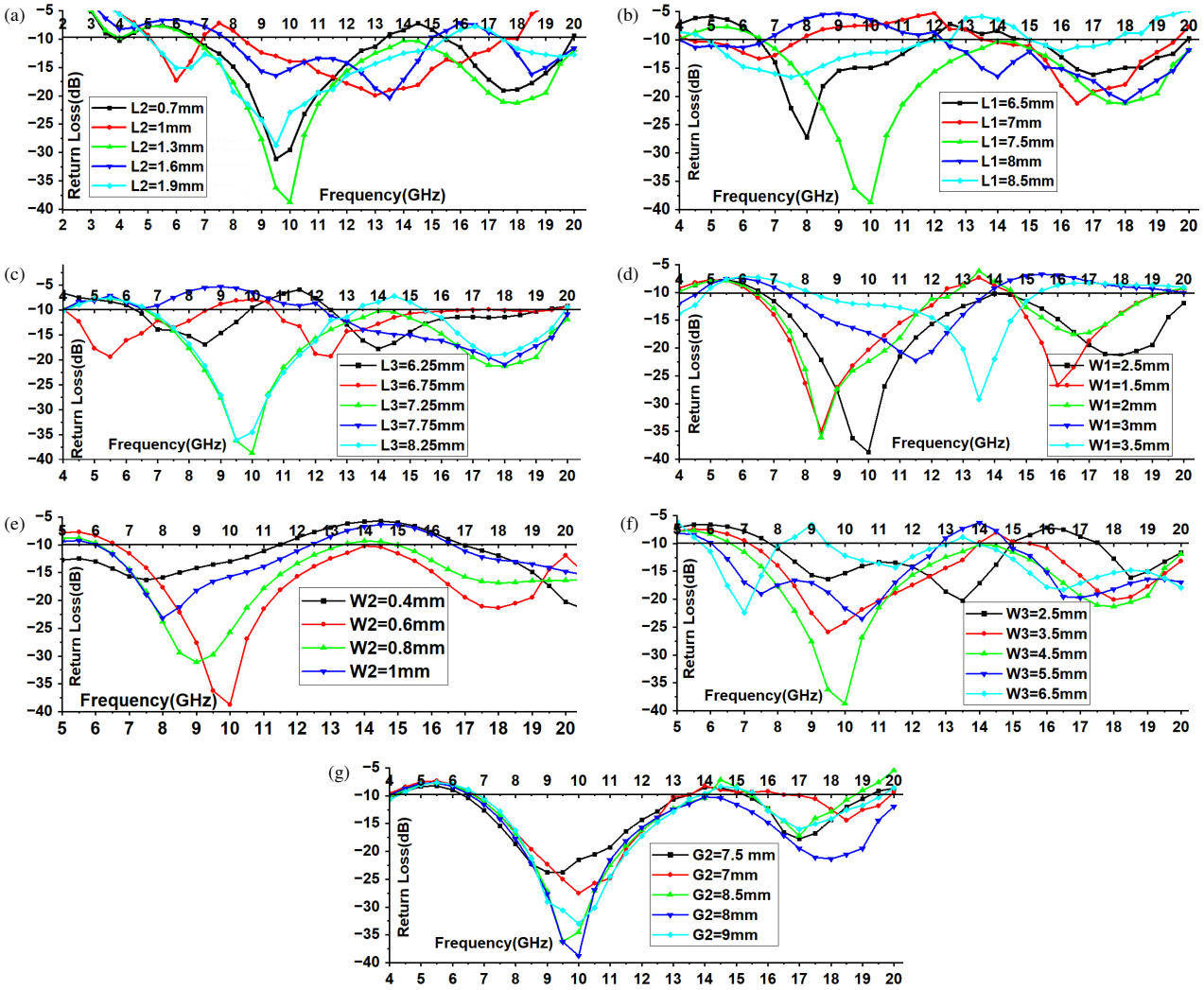

FIGURE 3. Simulated reflection coefficient due to variation of (a) $L1$, (b) $L2$, (c) $L3$, (d) $W1$, (e) $W2$, (f) $W3$, (g) $G2$.

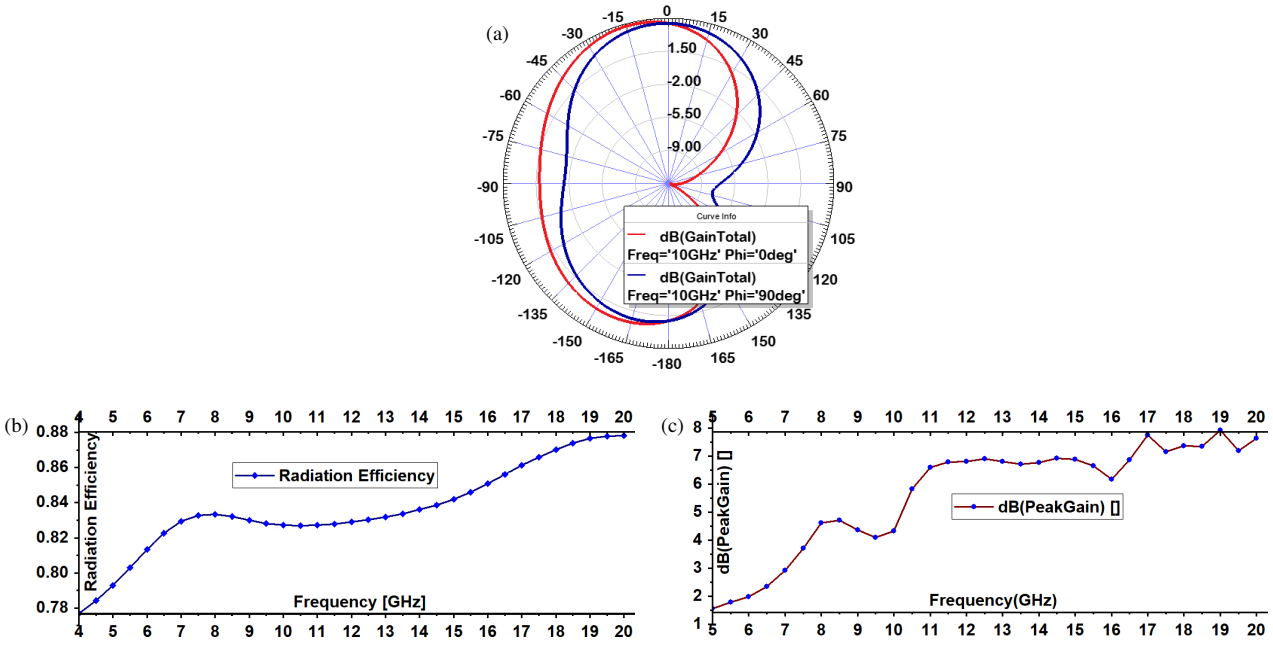

FIGURE 4. Radiation patterns 2-D at (a) 10 GHz, (b) radiation efficiency, (c) peak gain.

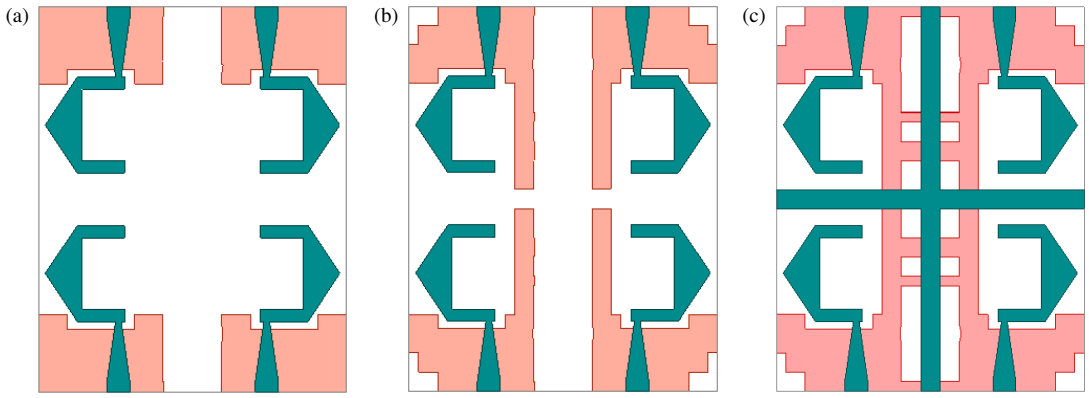

FIGURE 5. Evolution stages of the proposed MIMO antenna. (a) Ant-1, (b) Ant-2, (c) Ant-3.

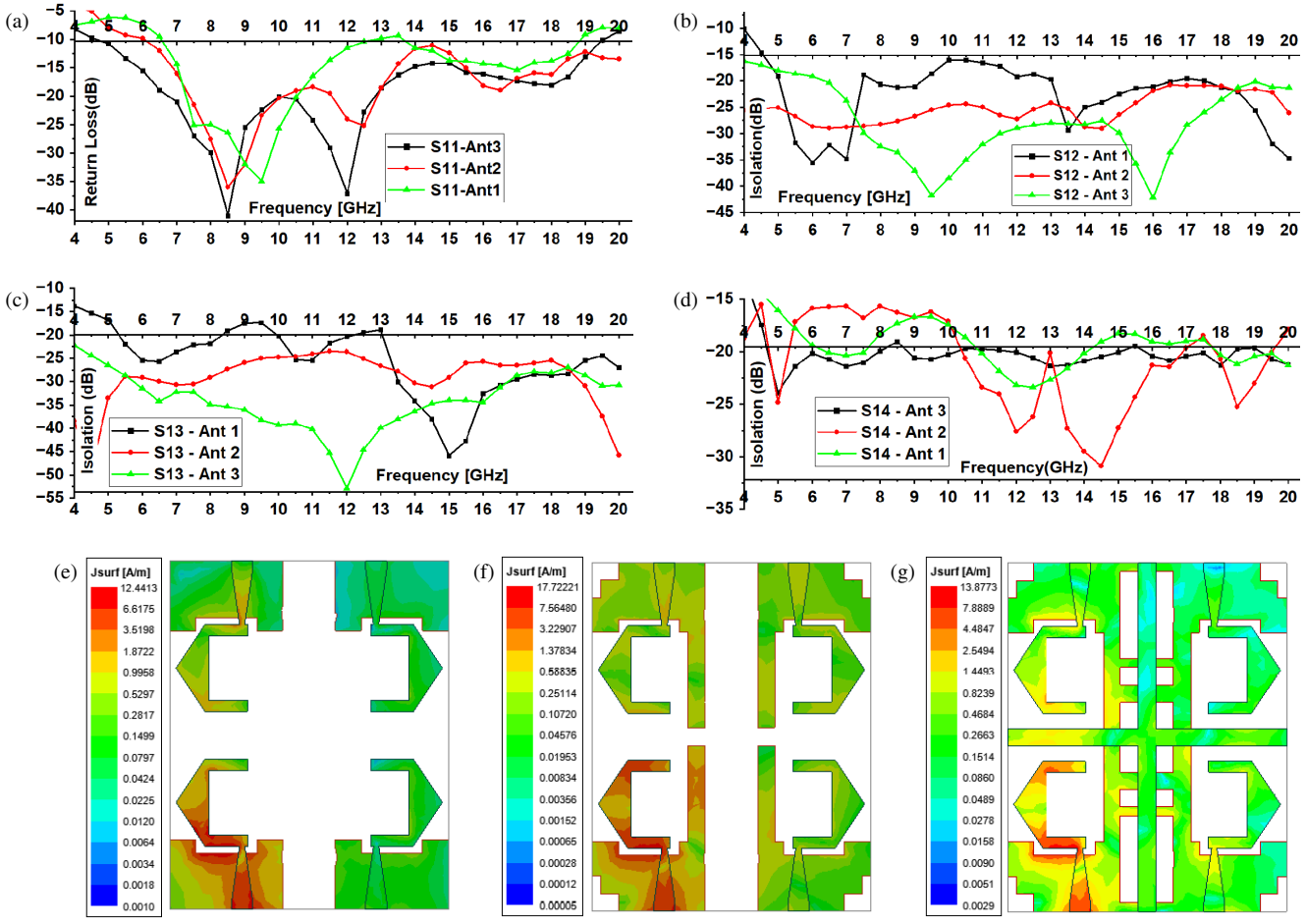

FIGURE 6. S-parameters at different phases (a) S_{11}, (b) S_{12}, (c) S_{13}, (d) S_{14}. Surface current distribution at 8.5 GHz, when port 1 is excited. (e) Unconnected ground plane (Ant-1). (f) Corner truncated with parallel stubs (Ant-2). (g) Connected ground plane with decoupling structure on the top of the antenna (Ant-3).

3. ANTENNA PERFORMANCE

3.1. Experimental Verification

3.1.1. S-Parameter Analysis (Compare Simulated and Measured)

A prototype of the proposed antenna was fabricated and tested using a vector network analyzer (Keysight N5224B PNA) in an anechoic chamber, as shown in Figs. 7(a)–7(d).

The comparison of simulated and measured S-parameters (S_{11}, S_{12}, S_{13}, S_{14}) in Fig. 8(a) show good agreement. The measured reflection coefficient (S_{11}) remains below -10 dB from 4.24 to 19.7 GHz, confirming a wide operational bandwidth of 15.48 GHz consistent with simulation. The isolation between antenna elements exceeds 20 dB across the band, as shown in Fig. 8(b), demonstrating the effective suppression of mutual coupling. Minor deviations between measured and sim-

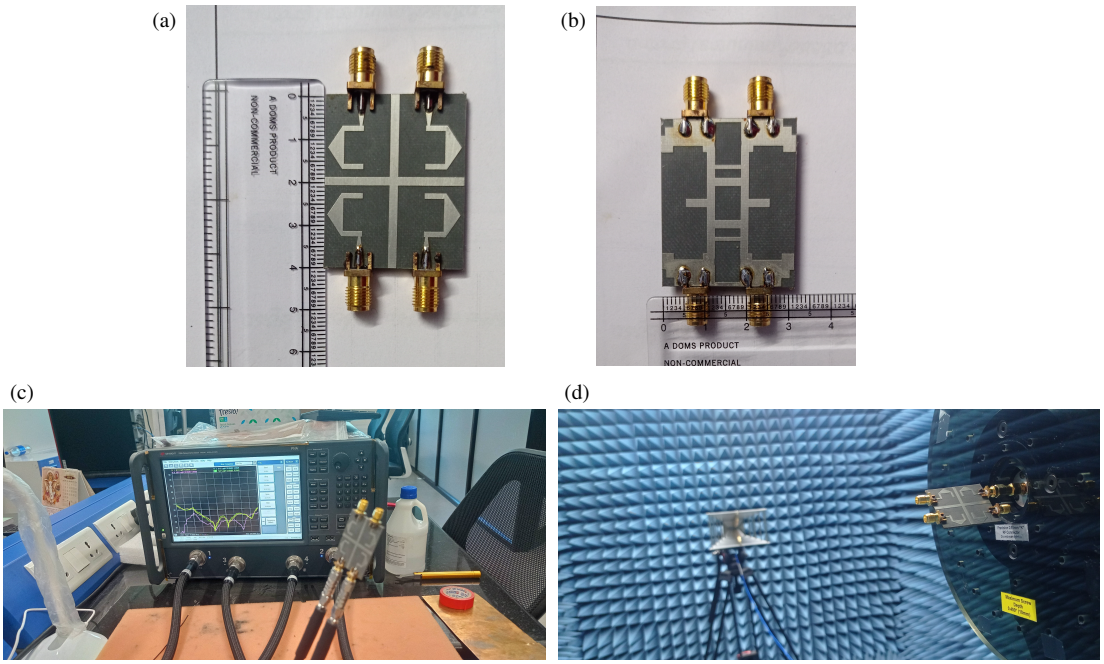

FIGURE 7. Fabricated prototype. (a) Radiating patch. (b) Ground. (c) S-parameters measurement using vector network analyzer. (d) Radiation characteristics measurement using anechoic chamber.

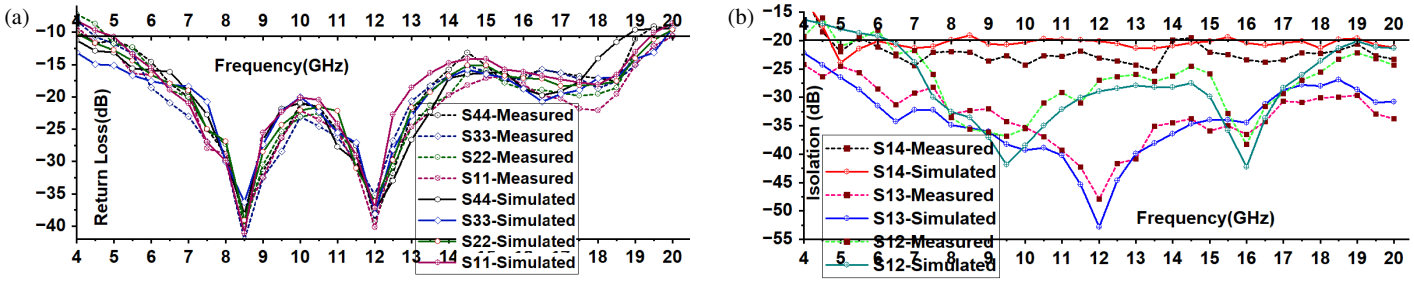

FIGURE 8. Comparison of simulated and measured S-parameters. (a) Return loss. (b) Isolation.

ulated results are attributed to connector losses, fabrication tolerances, and measurement setup limitations.

3.1.2. Radiation Characteristics (Compare Simulated and Measured)

Figures 9(a)–9(d) show the simulated and measured 2D radiation patterns of the antenna for co- and cross-polarizations at 8.5 and 12 GHz. At 8.5 GHz, cross-polarization levels in both E- and H-planes are well suppressed relative to co-polarization, indicating good polarization purity. Although some distortion appears at 12 GHz, the antenna maintains consistent co-polarized gain and acceptable performance, confirming its effectiveness as a wideband radiator.

3.1.3. Gain and Efficiency

Figures 10(a) and 10(b) show the simulated and measured peak gains and radiation efficiencies across 4.24–19.7 GHz. The measured peak gains are 4.3 dB at 10.5 GHz and 4.5 dB at 12 GHz, with efficiency ranging from 83% to 86.5%. The slightly higher simulated gain is attributed to measurement uncertainties and environmental variations.

3.1.4. Diversity Performance (ECC and DG)

Diversity performance was evaluated using envelope correlation coefficient (ECC) and diversity gain (DG). ECC, which measures pattern similarity between antenna elements, should be below 0.5 for practical use. In the proposed design, both simulated and measured ECC values remain under 0.02 across the band, as shown in Fig. 11(a), confirming excellent isolation.

DG, representing link reliability from independent fading paths, ideally approaches 10 dB. As shown in Fig. 11(b), the proposed antenna consistently achieves values above 9.975 dB, verifying strong diversity performance.

3.1.5. Channel Capacity Loss (CCL) and TARC Analysis

The channel capacity of a MIMO system ideally increases with the number of elements, but channel correlation introduces capacity loss, quantified by channel capacity loss (CCL). For practical designs, CCL should remain below 0.4 bits/s/Hz. As shown in Fig. 12(a), the proposed antenna achieves simulated and measured CCL values below 0.325 bits/s/Hz across the band.

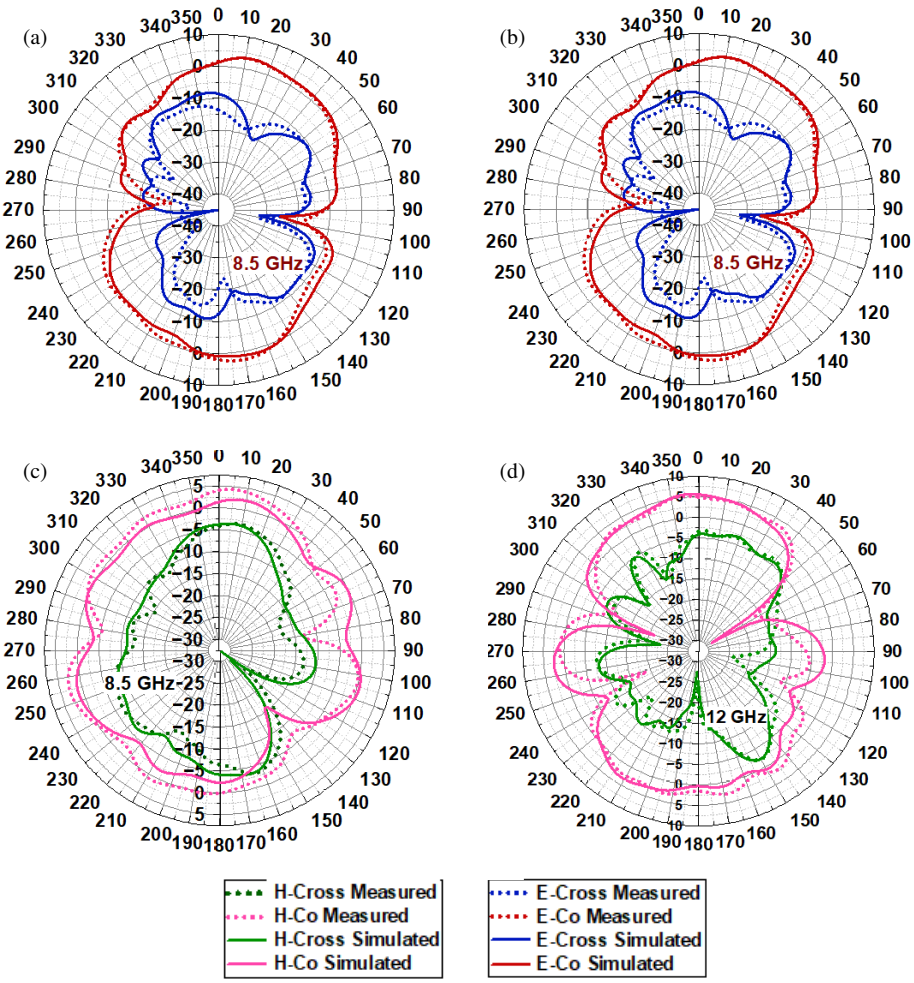

FIGURE 9. Simulated and measured polar radiation patterns: E-plane $\phi = 0°$) — co and cross (a) at 8.5 GHz, (b) at 12 GHz H-plane $\phi = 9°$) — co and cross, (c) at 8.5 GHz, (d) at 12 GHz.

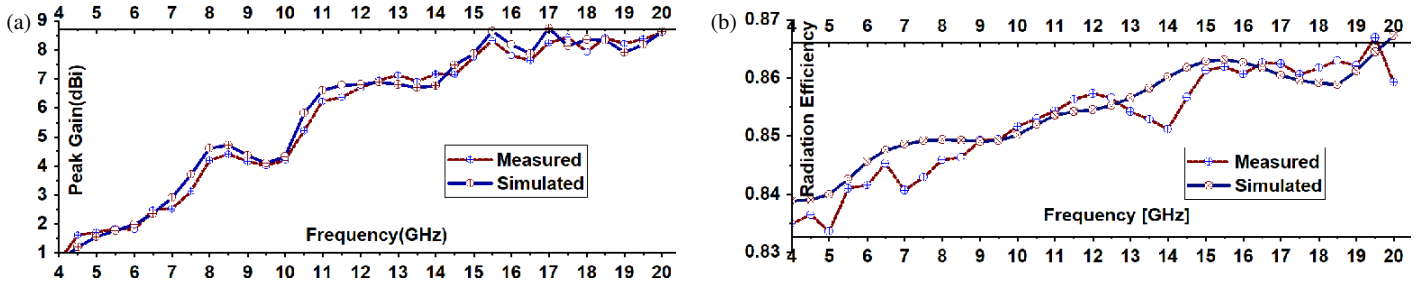

FIGURE 10. Simulation vs measurement of proposed MIMO antenna. (a) Peak gain (dBi). (b) Radiation efficiency.

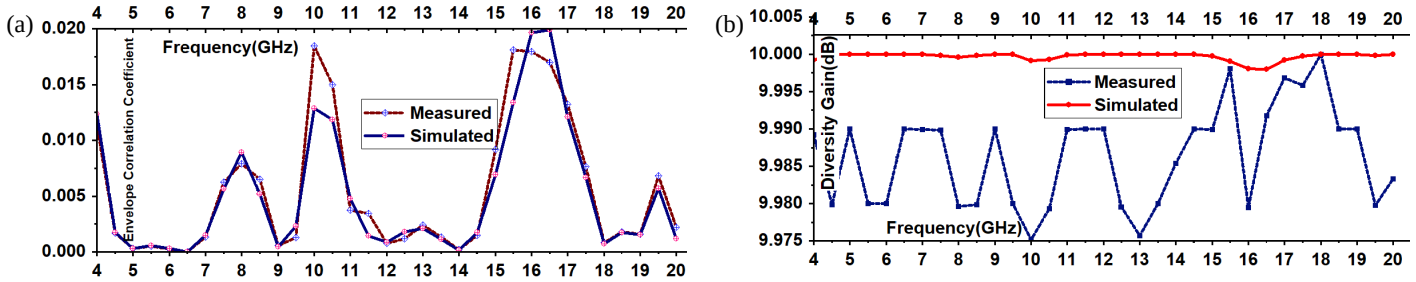

FIGURE 11. Simulation vs measurement, (a) envelope correlation coefficient, (b) diversity gain.

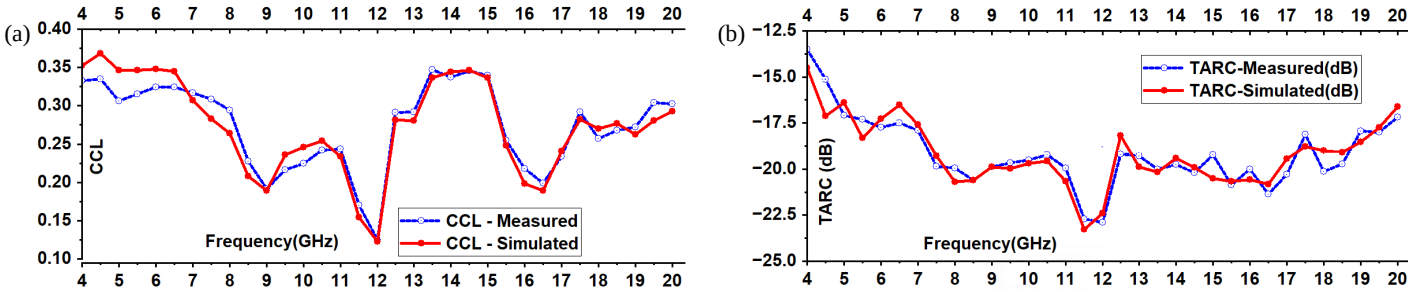

FIGURE 12. Simulated and measured (a) channel capacity loss, (b) total active reflection coefficient.

TABLE 2. Performance comparison of the proposed antenna with reported UWB/MIMO designs.

Ref.	Antenna Size (mm^3)	N.P	Substrate	Bandwidth (GHz)	Gain (dBi)	Isolation (dB)	ECC	RE (%)	TARC-dB	CCL	P.Y
[3]	$44 \times 44 \times 1.6$	4	FR4	2.95–10.8 N-1-5.1–5.9	2.4 to 4.0	< -15.5	< 0.04	70–82	–	–	2017
[4]	$40 \times 22 \times 1.6$	2	FR4	3.1–11.2 N1 −3.3–3.9 N2-4.9–5.9	2 to 5.1	< -15	< 0.002	90–96	–	–	2020
[5]	$39 \times 30 \times 0.8$	2	RT5880	2.3–20	0.5–6.2	< -22	< 0.001	70–98	−5 to −12	–	2024
[6]	$50 \times 50 \times 1.6$	4	Rogers R04003	3–20 N1-3.3–4.2 N2-4.5–5.5	0.5–4	< -15	< 0.1	–	–	< 0.4	2022
[7]	$40 \times 40 \times 1.6$	4	FR-4	3.1–14	5.5	< -18	< 0.012	> 89	–	< 0.29	2022
[8]	$36 \times 36 \times 0.8$	4	FR-4	2–11.08	3.5–6.5	< -15	< 0.13	70–90	−25 to −60	–	2024
[9]	$20 \times 20 \times 1$	2	RT5880	21.5–28.5	8.1(avg)	< -29	< 0.4	> 81	< -10	–	2024
[10]	$20 \times 20 \times 1$	2	RT5880	28–56	8.9(avg)	< -25	< 0.3	> 67	< -10	–	2024
[21]	$30.5 \times 20.5 \times 1.6$	2	FR4	3.1–11.85	2.7–3.8	< -20	< 0.05	> 81	–	< 0.02	2024
[22]	$25 \times 36 \times 1.6$	2	FR4	2.74–14.8	2–5.4	< -20	< 0.03	73–96	< -30	< 0.03	2024
[23]	$170 \times 80 \times 1.6$	2	FR4	3–6	3.1–3.8	< -25	< 0.01	–	–	–	2022
[24]	$62 \times 60.5 \times 1.6$	4	FR4	3.5–11	3.5 to 5.5	< -20	< 0.01	70–90	–	–	2023
[25]	$21 \times 27 \times 0.8$	2	FR4	3–11 N1-3.5–4 N2-4.8–5.2	0.5–5	< -15	< 0.02	72–90	–	–	2022
[26]	$25 \times 39 \times 1.6$	2	FR4	2.9–10.6	0.4–6.1	< -20	< 0.02	> 90	−10 to −20	< 0.25	2025
[27]	$38 \times 26 \times 1.6$	2	FR4	3.14–6.27	2–3.25	< -15	< 0.026	90–98	−12 to −25	–	2025
[28]	$39 \times 39 \times 0.8$	4	FR4	2.54–10.74 N1-3.3–4.9	1.3–3.9	< -15	< 0.3	76–92	–	–	2024
P.W	$40 \times 32 \times 1.2$	4	RT5880	4.24–19.70	1–8.5	< -22	< 0.02	83–86.5	−12 to −24	< 0.325	

- Ref. — References, N.P — No. of Ports, N — Notch band, ECC — Envelope Correlation Coefficient, DG — Diversity Gain, RE — Radiation Efficiency, TARC — Total Active Reflection Coefficient, CCL — Channel Capacity Loss, P.Y — Published Year, P.W — Proposed Work.

Figure 12(b) presents the total active reflection coefficient (TARC), defined as the ratio of reflected to incident power under multiport excitation. The antenna maintains excellent matching, with TARC values below −13 dB across the operating band.

3.1.6. Performance Comparison

Table 2 compares the antenna in terms of overall size, bandwidth, peak gain, ECC, and DG with previous designs.

4. CONCLUSION

A compact four-element monopole UWB MIMO antenna with a reflecting stub has been proposed, achieving wideband operation from 4.24 to 19.70 GHz. Parametric optimization was carried out to minimize radiator size while maintaining close element spacing, with high isolation (better than -20 dB) achieved through the reflecting stub and connected ground plane. The design demonstrates strong agreement between simulated and measured results for S-parameters and radiation patterns, while sustaining low ECC (< 0.02), high diversity gain (> 9.97 dB), low channel capacity loss (CCL < 0.0325), and favorable total active reflection coefficient (TARC between -12 and -24 dB). These outcomes confirm the antenna's robustness for MIMO performance. The proposed design is suitable for compact and high-density integration in wideband communication systems, with potential applications in sub-6 GHz 5G NR (n79), WLAN/Wi-Fi, X-band radar and radio navigation, and Ku-band satellite communication. Future work may explore further miniaturization and reconfigurable features to enhance adaptability across multi-standard platforms.

REFERENCES

[1] Kumar, O. P., P. Kumar, T. Ali, P. Kumar, and S. Vincent, "Ultrawideband antennas: Growth and evolution," *Micromachines*, Vol. 13, No. 1, 60, 2022.

[2] Dave, U. R., S. S. Modasiya, A. J. Dave, and R. M. Patel, "Progressions in ultra-wideband antenna design: A comprehensive overview of innovative strategies and real-world implementations," *SSRG International Journal of Electronics and Communication Engineering*, Vol. 11, No. 5, 139–154, 2024.

[3] Liu, Y.-Y. and Z.-H. Tu, "Compact differential band-notched stepped-slot UWB-MIMO antenna with common-mode suppression," *IEEE Antennas and Wireless Propagation Letters*, Vol. 16, 593–596, 2017.

[4] Devana, V. N. K. R. and A. M. Rao, "A novel dual band notched MIMO UWB antenna," *Progress In Electromagnetics Research Letters*, Vol. 93, 65–71, 2020.

[5] Khedr, A. A., B. E. Elnaghi, and A. M. Mohamed, "Design of a compact dual port 2×1 ultra-wideband MIMO antenna for radio frequency energy harvesting based on four "A" shaped slots," *Progress In Electromagnetics Research M*, Vol. 128, 41–49, 2024.

[6] Saritha, V. and C. Chandrasekhar, "A compact wide band MIMO antenna with quadruple notches in UWB," *Progress In Electromagnetics Research M*, Vol. 108, 237–247, 2022.

[7] Suresh, A. C. and T. S. Reddy, "A flower shaped miniaturized 4×4 MIMO antenna for UWB applications using characteristic mode analysis," *Progress In Electromagnetics Research C*, Vol. 119, 219–233, 2022.

[8] Ren, W., Z.-G. Wang, M. Yang, J. Zhou, and W.-Y. Nie, "Design of a simple four-port UWB-MIMO antenna based on a fan-shaped isolator," *Progress In Electromagnetics Research M*, Vol. 126, 117–126, 2024.

[9] Bhattacharya, A., "Design, fabrication, and measurement of a miniaturized MIMO antenna applicable for 5G communication," *International Journal of Microwave and Wireless Technologies*, Vol. 16, No. 4, 567–578, 2024.

[10] Bhattacharya, A., B. Roy, A. De, U. Chakraborty, and S. Mallik, "Extended investigations on a compact, isolation enhanced, printed MIMO antenna for higher band 5G," *Wireless Personal Communications*, Vol. 134, No. 2, 1093–1117, 2024.

[11] Sharma, M. K., M. Kumar, J. P. Saini, S. Sukla, and N. Bhati, "UWB-MIMO diversity antenna for next generation wireless applications," in *2016 3rd International Conference on Computing for Sustainable Global Development (INDIACom)*, 1528–1532, New Delhi, India, 2016.

[12] Devana, V. N. K. R., S. C. Sekhar, V. L. N. P. Ponnapalli, G. S. Reddy, N. Radha, *et al.*, "A compact MIMO antenna for GPS/PCS/Bluetooth wireless applications," in *2023 3rd International Conference on Intelligent Technologies (CONIT)*, 1–4, Hubli, India, 2023.

[13] Ali, W. A. E. and A. A. Ibrahim, "A compact double-sided MIMO antenna with an improved isolation for UWB applications," *AEU — International Journal of Electronics and Communications*, Vol. 82, 7–13, 2017.

[14] Khan, A. A., S. A. Naqvi, M. S. Khan, and B. Ijaz, "Quad port miniaturized MIMO antenna for UWB 11 GHz and 13 GHz frequency bands," *AEU — International Journal of Electronics and Communications*, Vol. 131, 153618, 2021.

[15] Devana, V. N. K. R. and A. M. Rao, "An octagonal shaped MIMO UWB antenna with dual band notched characteristics," in *Intelligent Communication Technologies and Virtual Mobile Networks*, 599–606, 2019.

[16] Deng, J.-Y., L.-X. Guo, and X.-L. Liu, "An ultrawideband MIMO antenna with a high isolation," *IEEE Antennas and Wireless Propagation Letters*, Vol. 15, 182–185, 2015.

[17] Kang, L., H. Li, X. Wang, and X. Shi, "Compact offset microstrip-fed MIMO antenna for band-notched UWB applications," *IEEE Antennas and Wireless Propagation Letters*, Vol. 14, 1754–1757, 2015.

[18] Ma, L., Z. Shao, J. Lai, C. Gu, and J. Mao, "A compact dual-decoupling scheme for aperture-coupled and probe-fed closely spaced wideband microstrip antennas," *IEEE Transactions on Antennas and Propagation*, Vol. 71, No. 11, 9072–9077, Nov. 2023.

[19] Devana, V. N. K. R. and A. M. Rao, "A compact flower slotted dual band notched ultrawideband antenna integrated with Ku band for ultrawideband, medical, direct broadcast service, and fixed satellite service applications," *Microwave and Optical Technology Letters*, Vol. 63, No. 2, 556–563, 2021.

[20] Devana, V. N. K. R., N. Radha, P. Sunitha, F. N. Alsunaydih, F. Alsaleem, and K. Alhassoon, "Compact MIMO UWB antenna integration with Ku band for advanced wireless communication applications," *Heliyon*, Vol. 10, No. 5, e27393, 2024.

[21] Pandya, K., T. Upadhyaya, V. Sorathiya, U. Patel, A. Pandya, and F. A. Al-Zahrani, "Highly isolated electrically compact UWB MIMO antenna for wireless communications applications," *Results in Engineering*, Vol. 24, 103082, 2024.

[22] Wang, Z., G. Song, W. Nie, M. Yang, C. Li, and M. Wang, "A racket-like UWB MIMO antenna with high isolation," *Progress In Electromagnetics Research C*, Vol. 144, 159–168, 2024.

[23] Sharma, R., R. Khanna, and G. Kapur, "Design of metamaterial loaded wideband sub-6 GHz 2×1 MIMO antenna with enhanced isolation using characteristic mode analysis," *Wireless Personal Communications*, Vol. 134, No. 3, 1713–1736, 2024.

[24] Abdelghany, M. A., M. F. A. Sree, A. Desai, and A. A. Ibrahim, "4-port octagonal shaped MIMO antenna with low mutual coupling for UWB applications," *Computer Modeling in Engineering & Sciences*, Vol. 136, No. 2, 1999–2015, 2023.

[25] Wu, L., X. Cao, and B. Yang, "Design and analysis of a compact UWB-MIMO antenna with four notched bands," *Progress In Electromagnetics Research M*, Vol. 108, 127–137, 2022.

[26] Thotakura, H., R. Gogineni, K. S. Rao, C. K. Kumar, R. B. Sadineni, and S. Mandava, "A miniaturized highly isolated two port triple band-notched UWB MIMO antenna verified by characteristic mode analysis," *Progress In Electromagnetics Research C*, Vol. 160, 133–142, 2025.

[27] Thanki, P., T. Upadhyaya, U. Patel, K. P. Kaur, K. Pandya, D. Patel, and V. T. Patel, "Compact wideband two port MIMO antenna with high isolation for wireless applications," in *2025 Fifth International Conference on Advances in Electrical, Computing, Communication and Sustainable Technologies (ICAECT)*, 1–5, Bhilai, India, 2025.

[28] Kaur, H., H. S. Singh, and R. Upadhyay, "Design and analysis of planar four-port UWB-MIMO antenna with band-rejection capability," *International Journal of Microwave and Wireless Technologies*, Vol. 16, No. 1, 127–139, 2024.